

Bow-Shock Instability around an Edged Ballistic Object in a Low-Gamma Gas

Yosuke Sato¹
Kanako Yasue²
Takamasa Kikuchi³
Kiyonobu Ohtani⁴
Naofumi Ohnishi⁵

¹Department of Aerospace Engineering, Tohoku University
Sendai, 980-8579
Japan

yosato@rhd.mech.tohoku.ac.jp

²Aerospace Research and Development Directorate
Japan Aerospace Exploration Agency
Chofu, 182-8522
Japan

yasue@chofu.jaxa.jp

³Institute of Fluid Science, Tohoku University
Sendai, 980-8577
Japan

kikuchi@edge.ifs.tohoku.ac.jp

⁴Institute of Fluid Science, Tohoku University
Sendai, 980-8577
Japan

ohtani@edge.ifs.tohoku.ac.jp

⁵Department of Aerospace Engineering, Tohoku University
Sendai, 980-8579
Japan

ohnishi@rhd.mech.tohoku.ac.jp

Abstract

Bow-shock instability observed in a low γ flow was investigated by three-dimensional numerical simulation with a circular cone. We designed experiments based on the numerical results in order to validate our numerical results and demonstrate that bow shock wave is unstable in a low γ gas with the edged body. The experimental results show that bow shock becomes unsteady and unstable in the proposed condition, and our numerical prediction was validated.

Key words: bow-shock instability, discontinuous Galerkin method, ballistic range.

Introduction

Some problems caused by shock waves in a supersonic flight, such as wave drag, heat load, and sonic boom, prevent from realizing affordable supersonic transports, although many attempts have been made to conquer them. In order to propose a new shock wave application, which is different from existing methods based on steady shock waves, we have focused on an instability of bow shock wave. Actively using this instability, the shock wave itself may be weakened; therefore, wave drag, heat load, and sonic boom are also reduced all

together. Moreover, understanding dynamics of the detached shock wave is very important for evaluating heat flux for a re-entry vehicle.

In some experiments using a ballistic range, the results suggest that the bow shock wave may be unstable in low- γ gas[1, 2, 3], as shown in Fig. 1[1, 2]. From experimental results of Baryshnikov et al., it was concluded that the instability occurs depending on Mach number, ambient gas pressure, and curvature of a blunt body. They also mentioned that a cause of the instability is chemical reaction in the shock layer. However, since it is difficult to analyze the flowfield behind the shock wave in the experiments, the mechanism of the instability has not yet been revealed. So, it is expected that computational fluid dynamics (CFD) enables a detailed analysis of the instability and clarifying the cause of it.

On the other hand, in CFD with a strong shock wave, most of shock-capturing schemes become unstable when the shock wave is parallel to computational grids; this is so-called carbuncle phenomenon[4]. The carbuncle phenomenon also occurs depending on various factors such as flow conditions, computational grids, and flux function schemes. Therefore, an appropriate computational condition is required to extract the physical instability by keeping off the carbuncle phenomenon. Even now, however, a main factor of this numerical instability is not revealed, in spite of numerical and theoretical studies. Therefore, in analysis of shock-wave instabilities, we must assess the carbuncle phenomenon for the obtained results in a careful way.

We have conducted three-dimensional computations with Discontinuous Galerkin (DG) method[5] on unstructured grids in order to explore mechanism of the bow-shock instability which was observed in Freon by ballistic experiments more than thirty years ago. We have examined robustness of Riemann solvers against the carbuncle phenomenon in the condition we want[6] and employed a AUSM family scheme in the present paper. Moreover, through analysis with semi-ellipsoids of large aspect ratios, we obtained computational grids which seem to cause less numerical instability. With the above knowledge, we investigated dependency of the instability on body shapes[7]. As a result, our numerical simulations show that the instability appears around an edged object such as base of cone or cylinder with neither chemical reaction nor viscous effect when specific heat ratio of main stream is lower than the critical one. This instability is likely to be physical one, but the existence of the carbuncle phenomenon does not enable us to conclude that the numerical results are really caused by physical origins.

Therefore, we have designed experiments with ballistic range in a condition based on our numerical results, such as body shape, freestream Mach number, and specific heat ratio. The experimental results will validate our numerical simulations and may consequently suggest a better experimental design by a suitable numerical modeling like hypersonic effects which can describe the realistic bow-shock instability in the laboratory.

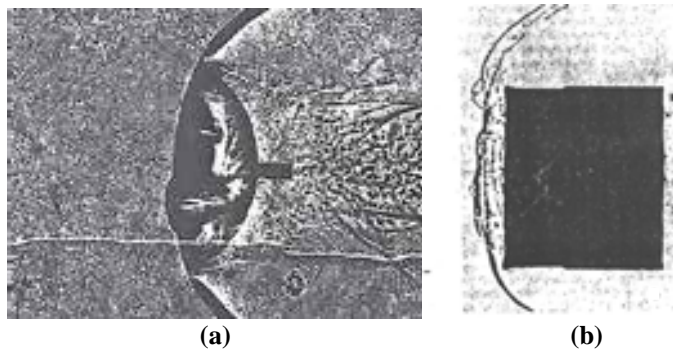


Fig. 1 Experimentally observed unstable bow shock waves[1, 2].

Numerical Simulation

The experimentally observed instability is three-dimensional phenomenon, and the body shape may have a significant role on inducing the instability. Therefore, we use three-dimensional unstructured grids which have geometrical flexibility and are easy to change its configuration according to the body shape. Euler equations are solved by the DG method which is a kind of finite-element method and can achieve relatively high order of accuracy even on the unstructured grids. In this study, the spatial accuracy of the DG method is second-order, and we employ SLAU[8] method as a numerical flux function. For the time integration, two-stage TVD Runge-Kutta method[9] is used. We do not consider any chemistry behind the shock wave. As computational conditions, Mainstream Mach number changes from 1.0 to 10.0, ratio of specific heat varies from 1.0 to 1.4 with zero angle of attack. Moreover, CFL number is commonly set to 0.3, and prismatic computational cells were used in our simulations.

Experiment

Experiments were conducted with a ballistic range at the Institute of Fluid Science (IFS), Tohoku University in the single stage powder gun mode[10]. It consists of a powder chamber, acceleration tube with 15 mm in diameter and 3.0 m in length, and a test section with 1.66 m in diameter and 12 m in length. We set a test chamber (60 mm \times 145 mm \times 1500 mm) in the test section, and usage of a test gas can be greatly reduced by filling the gas only in the chamber with diaphragms. Schematics of the chamber part is shown in Fig. 2. High purity of the test gas is acquired by vacuuming the chamber before filling the gas. This optical setup for shadowgraph method is used with continuous light source (metal halide lamp, LS-M210, SUMITA, 210 W).

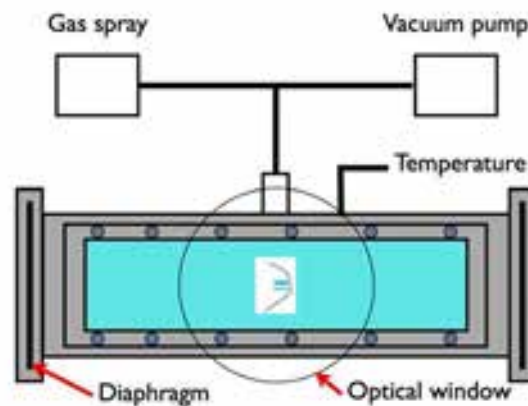


Fig. 2 Schematics of test chamber.

Results and Discussion

Dependency of Bow-Shock Instability on Body Shapes

Mach number distributions in subsonic region around a circular cone and circular cylinder are shown in Fig. [3] when γ is 1.01. Although the shock fronts become steady in both cases, a deformation of the shock front is observed with the circular cone. The asymmetric disturbances in the distributions are found for both cases. Additionally, the features of the shock deformation ahead of the circular cone resemble the ones obtained by the past experiments (Fig. 1 (a)). So, the observed instability may result from a physical origin.

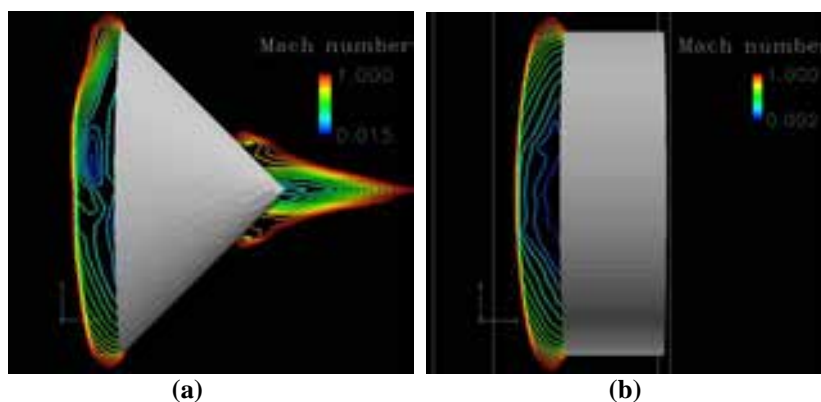


Fig. 3 Mach number distribution in subsonic region around (a) circular cone and (b) circular cylinder.

Assessment of carbuncle phenomenon

As mentioned above, it is known that a computed shock wave tends to unstable with strong shock wave. If the results with our simulation are numerical instability caused by numerical error, however, the wavelength of the

shock deformations should depend on the computational grids. So, we checked grid dependency of the obtained results. Three different grids were used, and the numbers of the cells are 375,436, 1,488,852, and 2,009,070, respectively. Figure 4 shows pressure distributions with these grid systems. Note that the freestream condition is $M = 3.9$, $\gamma = 1.05$. In all cases, comparable wavelength is predominant in the shock deformations, so this instability should be physical one. Since the scale of the wavelength is close to the cone radius, a characteristic length for the body may have an effect on determining it.

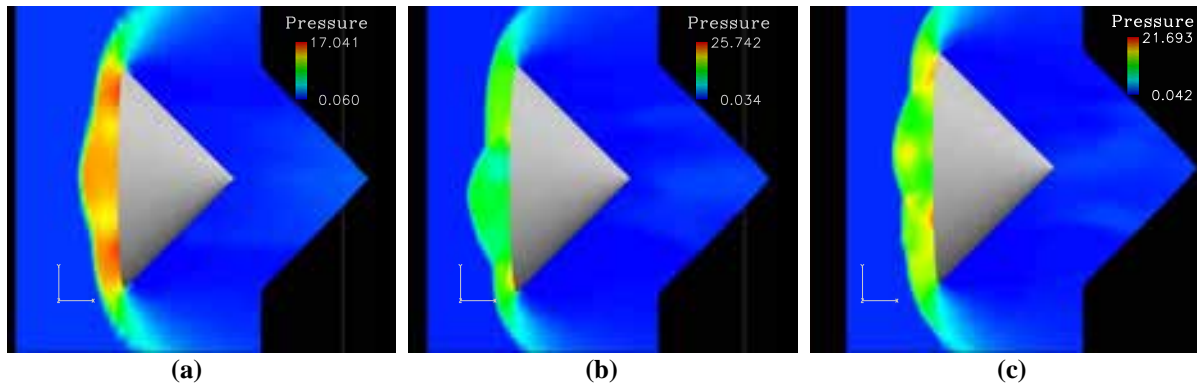


Fig. 4 Grid dependency of instability around (a) 375,436 cells, (b) 1,488,852 cells and (c) 2,009,070 cells.

Stability diagram in $\gamma - M$ plane

Figure 5 shows numerical results for parameters of γ and M . Blue symbols indicate the bow shock are unstable, and red stable. With the circular cone, a critical line for unstable bow is found in $\gamma - M$ plane. Generally, shock stand-off distance becomes small when γ is low and M is high. The narrow shock layer may make it unstable by an interaction between the shock front and vortices generated in the shock layer. The critical Mach number greatly changes at $\gamma = 1.2$. This suggests that not only the shock thickness but also vortex generation induced by large density ratio across the shock wave may affect this instability.

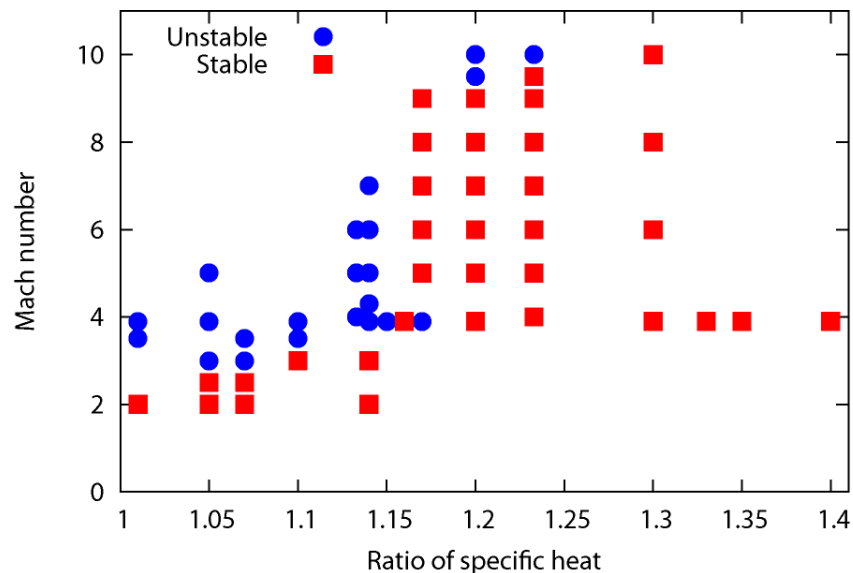


Fig. 5 Stability diagram in $\gamma - M$ plane.

Experimental Condition Based on Numerical Results

As a test gas, we use HFC-134a (CH_2FCF_3) which is generally used as a refrigerant gas. Specific heat ratio of this gas is 1.23, so the flight Mach number is set to 10 from Fig. 5. Because this gas is polyatomic, sound speed in it is relatively small and about 180 m/s at room temperature and atmospheric pressure. Therefore, injection

speed of the projectile is about 1.8 km/s when Mach is 10, and we can conduct an experiment in this condition using the ballistic range facility at IFS, Tohoku University. Note that HFC-134a is unbarnable and non-corrosive. Ozone depletion potential is also zero. Thus there is no need for special consideration under the experiment and for post-processing of the gas. Computed density distribution for the assumed condition is shown in Fig. 6. Deformation is found at the shock front, and this scale deformation can be observed by the resolution of the experiment.

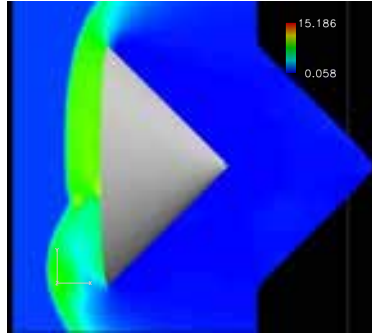


Fig. 6 Density distribution for the assumed condition.

Projectile

Figure 7 depicts a projectile used in the experiment. From the numerical assessment for body shape, we found that flowfield around the edge part of the cone is important for this instability[11]. Therefore, we use a projectile whose front part is cone with 45 degree edge like the simulation, and rear part is a cylinder of $\phi = 15$ mm which fits experimental device. The weight is about 4 g. We have confirmed that the deformation arises at the shock front even with different rear shapes by numerical simulations. Additionally, From the Mach number distribution in Fig. 3, it is obvious that the shape of the rear part does not affect flowfields in front of it. The front part is made of duralumin for withstanding severe heating due to hypersonic speed, and the rear part is polycarbonate.

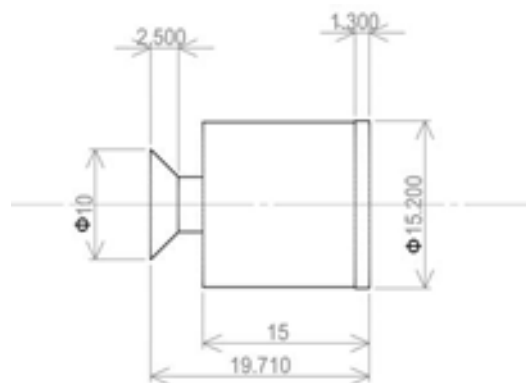


Fig. 7 Projectile shape.

Experimental results

Figure 8 depicts sequential shadowgraph images of the experiment. The projectile speed was estimated about 1.8 m/s ($M = 10.5$), and the angle of attack is zero. Time variation and deformation of the shock front ahead of the body is observed, which suggests the bow shock be unsteady and unstable in this condition. Note that the bow shock has a three-dimensional structure, so the front part of the body is not seen in these images. The shape of the shock front is deferent from numerical results. Some factors may affect this discrepancy. First, the flight Mach number is not the same as numerical simulation, and M does affect the shape of the shock front. Secondly, real gas effect such as dissociation due to severe temperature increase in a hypersonic shock may affect. The shock layer temperature reaches about 3,000 K; thus this effect may not be neglected. Moreover, other causes

are arguable, and more detailed analysis and simulations are needed. However, a principal objective of this experiment that validates the instability of bow shock wave was achieved. These results suggest that a main factor of bow-shock instability is likely pure hydrodynamic effect, although real gas effects could not be neglected in the real problem.

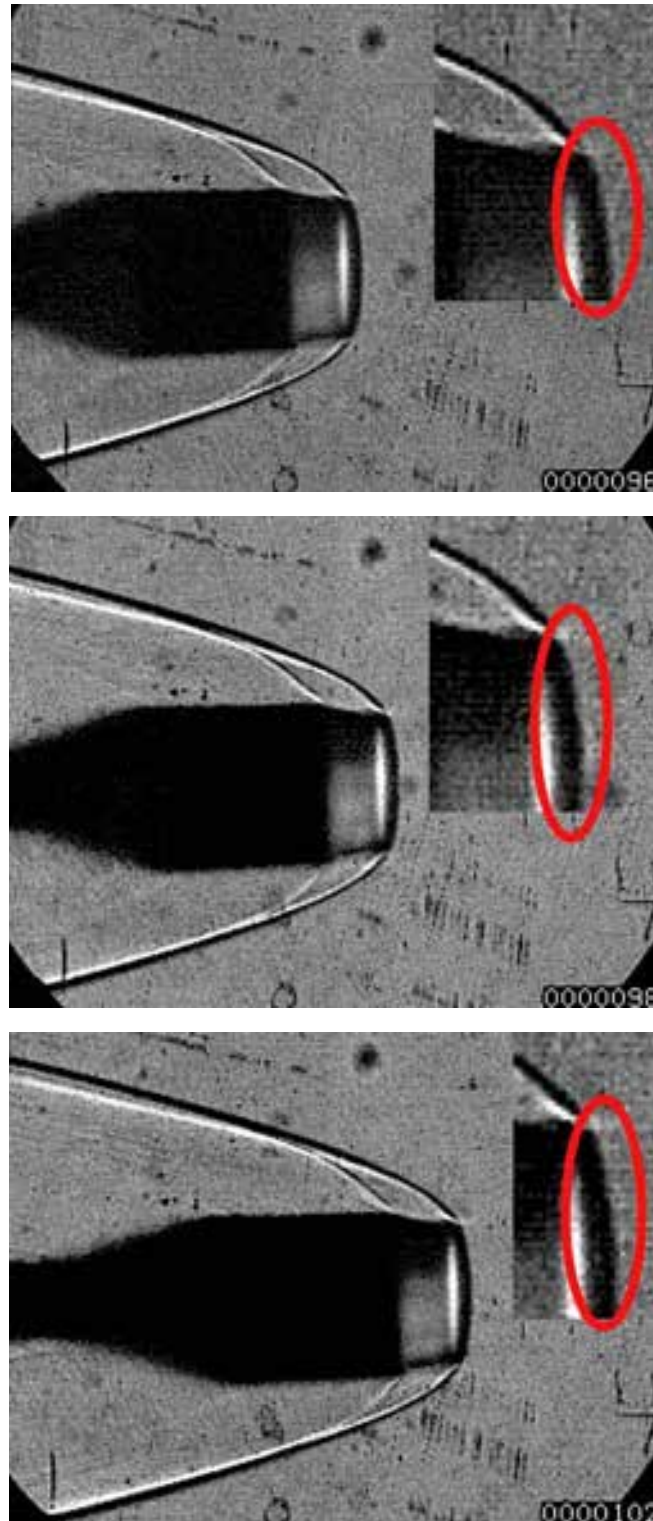


Fig. 8 Shadowgraph images of the bow shock around the projectile in the test gas. (a) $t = 0 \mu\text{s}$, (b) $t = 2 \mu\text{s}$, and (c) $t = 6 \mu\text{s}$.

Conclusions

Three-dimensional numerical simulations were conducted with DG finite-element method on unstructured grids, and bow-shock instability was reproduced with a circular cone in a low γ flow. Based on the numerical results, we designed an experiment to observe the instability in the laboratory in order to validate our results. The experimental results depicted that the bow shock wave in the condition can be unsteady and unstable. Therefore, our numerical results with Euler equations were validated to some extent, although the shock shape was different from the calculation. There are some factors for this discrepancy, such as real gas effect due to hypersonic speed and time variation of projectile speed or posture. However, the numerical and the experimental results suggest that the bow shock can become unstable by purely hydrodynamic effect. We will conduct further experiments and more detailed analysis by our numerical simulation validated in this experiment.

Acknowledgements

The authors would like to acknowledge Messrs. T. Ogawa, T. Ukai, and Y. Saito of Institute of Fluid Science, Tohoku University for their assistance in performing the present experiments.

References

- [1] A. S. Baryshnikov, A. P. Bedin, V. G. Maslennikov and G. I. Mishin, Stability of a bow shock. *Sov. Tech. Phys. Lett.*, **5**, 113-114 (1979).
- [2] A. S. Baryshnikov, Baroclinic turbulence of dissociating gas as a reason for instability of bow shock wave. *Phys. Scr.*, **T132**, 014007 (2008).
- [3] H. G. Hornung and P. Lemieux, Shock layer instability near the Newtonian limit of hypervelocity flows. *Physics of Fluids*, **13**, 8 (2001)
- [4] J. Quirk, A contribution to the great Riemann solver debate. *International Journal for Numerical Methods in Fluids*, **18**, 555 (1994).
- [5] B. Cockburn and C.-W. Shu, The Runge-Kutta discontinuous Galerkin method for conservation laws V: Multidimensional systems. *Journal of Computational Physics*, **141**, 199 (1998).
- [6] Y. Sato, Y. Suzuki, K. Yasue and N. Ohnishi, Three-dimensional simulation of bow-shock instability using discontinuous Galerkin method. *Proceedings of the 28th International Symposium on Shock Waves*, **1**, 1027, Springer (2011).
- [7] Y. Sato, K. Yasue and N. Ohnishi, Bow-shock instability with edged body in low- γ flow. *AIAA Paper*, 2012-2708 (2012).
- [8] E. Shima and K. Kitamura, On New Simple Low-Dissipation Scheme of AUSM-Family for All Speeds. *AIAA Paper*, 2009-136 (2009).
- [9] S. Gottlieb and C.-W. Shu, Total Variation Diminishing Runge-Kutta Schemes. *Mathematics of Computation*, **67**, 73 (1998).
- [10] D. Numata, Experimental study on hypervelocity impact phenomena at low temperatures with ballistic range, *Doctor thesis, Tohoku University* (2008)
- [11] Y. Sato, K. Yasue and N. Ohnishi, Numerical simulation of Bow-shock instability around circular cone. *Proceedings of 20th International Shock Interaction Symposium*, 157 (2012).